Atomic Structure of the Y-Complex of the Nuclear Pore

Kotaro Kelley[#], **Kevin E. Knockenhauer**[#], **Greg Kabachinski**, and **Thomas U. Schwartz**
Department of Biology, Massachusetts Institute of Technology Cambridge, MA USA.

[#] These authors contributed equally to this work.

Abstract

The nuclear pore complex (NPC) is the principal gateway for transport into and out of the nucleus. Selectivity is achieved through the hydrogel-like core of the NPC. The structural integrity of the NPC depends on ~15 architectural proteins, which are organized in distinct subcomplexes to form the >40 MDa ring-like structure. Here we present the 4.1 Å crystal structure of a heterotetrameric core element ('hub') of the Y-complex, the essential NPC building block, from *Myceliophthora thermophila*. Using the 'hub' structure together with known Y-complex fragments we built the entire ~0.5 MDa Y-complex. Our data reveal that the conserved core of the Y-complex has 6, rather than 7 members. Evolutionarily distant Y-complex assemblies share a conserved core that is very similar in shape and dimension, suggesting that there are closely related architectural codes for constructing the NPC in all eukaryotes.

INTRODUCTION

In all eukaryotic cells transcription and translation are physically separated between the nucleus and cytoplasm. This allows for distinct gene expression control mechanisms, for example in cell differentiation and development, unavailable to prokaryotes. Nuclear pore complexes (NPCs), which perforate the nuclear envelope and act as the main transport gate, therefore have a fundamental role in cellular homeostasis[1,2]. The NPC is a modular, donut-shaped assembly of ~30 different proteins (nucleoporins or nups), arranged in multiples of eight around a central axis that is aligned with the main transport channel[3]. Nups can be classified as (i) architectural nups, which form the stable scaffold of the NPC, (ii) peripheral nups with various degrees of mobility, and (iii) nups with the characteristic phenylalanine-glycine (FG)-repeat elements in disordered extensions that form the permeability barrier.

To gain mechanistic insight into NPC function, considerable effort has been undertaken to determine the NPC structure at high resolution. Due to its enormous size of ~40–120

MDa[4-6], this will ultimately only be possible with a combination of different visualization techniques, notably X-ray crystallography and cryo-electron microscopy.

One of the main architectural elements of the NPC is the Y-shaped complex, which is essential for NPC formation[7,8]. In *S. cerevisiae*, it is a 7-membered 575 kDa complex composed of Nup84, Nup85, Nup120, Nup133, Nup145C, Sec13 and Seh1[9] . Homologs for these 7 members are also found in humans, suggesting conservation within all opisthokonts[10-12]. It is widely believed that the Y-complex, together with the heteromeric Nic96 complex, forms the principal NPC scaffold[13-15]. Thus, the atomic structures of the assembled Y- and Nic96 complexes are important milestones toward understanding the NPC at the highest resolution. All 7 members of the Y-complex have been studied crystallographically, though only individually or as heterodimeric or trimeric complexes, and typically truncated[16-27]. The branch point or 'hub' of the Y-complex, where the two short arms and the long stalk meet, is structurally the least understood even though it is arguably the most important element (Fig. 1a).

Here we now report the structure of the Y-complex hub, which enables us to combine all the additional fragmentary structures into a highly accurate assembled structure of the Y-complex. We can show that the Y-complex structure is widely conserved among all eukaryotes. Species-specific additions to the Y-complex decorate, but do not principally alter the overall structure.

RESULTS

Structure of the Y-complex hub

We generated a series of structure-based expression constructs containing the elements of Nup120, Nup145C, and Nup85 that were known to directly interact with each other at the Y-complex hub[18,20,22,28]. In addition, these constructs were designed to overlap at least partially with the already structurally characterized Y-complex fragments. We succeeded in obtaining crystals of a heterotetrameric construct containing $Nup85_{257-1181}$, $Nup120_{952-1241}$, $Nup145C_{233-791}$, and Sec13 from the thermophilic fungus *Myceliophthora thermophila (mt)*, which diffracted to 4.1 Å resolution (Table 1). The structure was solved with a combination of molecular replacement and single anomalous dispersion (SAD) using selenomethionine-derivatized protein (see Methods for details). The crystals have a high solvent content (68%) and the structure has a comparatively high degree of positional disorder (Wilson B factor 144 $Å^2$). Despite the high Wilson B factor, we were able to properly assign the sequence to all four proteins within the assembled complex based on model building guided by selenomethionine positions, homology models, and phylogenetic considerations (Supplementary Table 1).

The overall structure of the heterotetramer is roughly V-shaped, composed of three helical units, Nup85, Nup120, and Nup145C, and a laterally attached β-propeller, Sec13 (Fig. 1b, Supplementary Fig. 1). Nup85 and Nup145C form the long sides of the 'V', while Nup120 is sandwiched between the two sides and acts as the main connector. Sec13 is bound to Nup145C as previously described in the Nup145C-Sec13-Nup84 structure from *Saccharomyces cerevisiae (sc)*[19,25], namely by the insertion of a seventh blade into its open,

6-bladed β-propeller. Viewed from the side, it is noticeable that the heterotetramer is substantially bent rather than flat (Fig. 1c). The overall dimensions of the complex are ~125 Å × ~140 Å × ~50 Å.

Nup85 and Nup145C belong to the ancestral coatomer element 1 (ACE1)-class of proteins. These proteins are characterized by a ~65kDa, tripartite helical segment composed of a crown, a trunk and a tail element, which adopts a characteristic fold-back structure involving ~30 α-helices[3,18]. ACE1 proteins are exclusively found in the NPC scaffold and the COPII vesicle coat[29]. The scNup85 and scNup145C fragments solved previously both lack the tail elements, which are present in this structure. These tail elements are in direct contact with Nup120. Even though the identity between the Mt and Sc sequences is low (14% for Nup85, 20% for Nup145C) (Supplementary Table 2, Supplementary Notes 1–4), the structures superpose well (Supplementary Fig. 2). Therefore, we assigned secondary structure elements in the Mt proteins in accord with the published Sc fragments[18,19]. Nup145C has 27 helices in total. Helices α1–α3 and α12–α20 form the trunk, α4–α11 the crown, and α21 to α27 the tail. The entire helical stack of Nup145C has a crescent shape. To stabilize the Sec13 interaction, we fused Sec13 N-terminally to 145C, similar to what was previously done for scSec13-Nup145C[19]. For this reason, our Nup145C construct is lacking 232 N-terminal, predicted-to-be disordered residues.

Nup85 has 33 helices in total. Helices α1–α3 and α12–α20 form the trunk, α4–α11 the crown, and α21 to α30 the tail. Compared to mtNup145C, the mtNup85 tail domain is longer, and contains 4 additional helices. In *S. cerevisiae*, Nup85 binds Seh1 very similarly to Nup145C binding Sec13, i.e. via an insertion blade that closes the open, 6-bladed β-propeller. Although Sordariomycota, including *M. thermophila* and *C. thermophilum*, also contain a recognizable Seh1 homolog, it does not bind to Nup85[30]. The structure now reveals that mtNup85 lacks the essential Seh1-binding site, i.e. the insertion blade. Instead, it contains an additional N-terminal helix α0 (Fig. 1, Supplementary Fig. 3), incompatible with Seh1 binding. In light of this observation, we suggest that Seh1 is not a member of the conserved core of the Y-complex. This core is a heterohexamer rather than a heteroheptamer. The presence of an Seh1 homolog in Sordariomycota is likely due to its function in the GATOR(SEA) complex[31,32].

The C-terminal fragment of Nup120 contains 10 helices (α23–α29,α29a,α29b,α30), 8 of which form a regular stack. This stack superimposes very well (RMSD 2.2 Å over 135 Cα positions) with the C terminus of Nup120 from *S. pombe*[22]. The C-terminal mtNup120 element is wedged between the tail domains of Nup85 and Nup145C, and forms the core of the hub. The interface between Nup120 and Nup85 buries a ~940 Å^2 surface, while the Nup120-Nup145C interface measures ~1700 Å^2. The Nup120-Nup85 interface includes helices α27 and α29 from Nup120 and helices α28 and α30 from Nup85. This arrangement generates a tightly packed four-helix bundle between the two proteins, likely explaining the high affinity of both proteins for each other. In comparison, the Nup120-Nup145C interface is more complicated, with two major elements contributing contacts. One part of the binding interface is generated by the terminal helix α27 of Nup145C that runs along the narrow ridge of the Nup120 C-terminal helical stack. Helices α29a and α29b of Nup120 are outside of the C-terminal stack and clamp down Nup145C, as they are positioned on the outward-

facing side of the molecule, thereby forming a second interaction site. Helices α29a+b are not conserved, but appear to be specific for Sordariomycota (Supplementary Note 3).

Sec13 is placed right in the neck of the V-shaped molecule, with contacts to all three helical proteins. The contact area with mtNup145C is largest and very similar to the homologous structure of scNup145C[19,25]. In addition to the close contacts with the insertion blade, the top surface of the Sec13 β-propeller binds the trunk of the Nup145C-ACE1 element. The Sec13-Nup120 contacts are established through interactions between blades 1 and 2 of Sec13, and the very C-terminal helix α30 of Nup120. Finally, contacts between Sec13 and Nup85 are few, but nonetheless likely important. Taken together, it appears as if the Sec13 position helps to rigidify the interaction between the three helical elements.

Fitness analysis

To evaluate the importance of the hub interface *in vivo,* we used a fitness test in *S. cerevisiae.* C-terminal truncations of the last helix of Nup85, Nup120, and Nup145C, were designed to selectively disrupt the mapped interfaces between the three helical proteins. The Nup85 α30 mutant had the most severe phenotype and showed drastically reduced growth (Fig. 2). Nup145C α27 and Nup120 α30 have progressively milder phenotypes. Nup85 α30 almost phenocopies the lethal Nup85 knockout[33], suggesting that the Nup85-Nup120 interaction is critical for NPC assembly. For Nup120 and Nup145C, it is likely that the mapped interfaces are not the exclusive elements that integrate these proteins into the NPC, but that additional contacts exist. The N-terminal extension of Nup145C, past the Sec13 insertion blade and not part of our structure, is likely to play a role in this. However, contacts to other scaffold nucleoporins need to be considered as well. Additionally, while we did not formally quantify the protein levels or test the fold retention of the individual truncated proteins, based on previous *in vivo*[28] and *in vitro*[18,20,22,34] experiments, we can assume that our specific truncations are folded correctly and expressed at wild type levels.

Composite high-resolution structure of the Y-complex

With the heterotetrameric hub assembly in hand we set out to build a complete high-resolution, composite structure of the entire Y-complex. The structures of full-length Nup120[22] and Nup84-Nup145C- Sec13[19] contain overlapping elements with the hub structure, 19 kDa and 85 kDa in size, respectively, and were superposed with high confidence (Supplementary Fig. 4). This generated a heteropentameric complex, in which Nup84 is the preliminary terminal fragment of the long stalk of the Y. Nup84 is an ACE1 protein, but the published structure lacks the tail domain (residues 443–724) that interacts with Nup133. However, the structure of most of the tail domain of Nup107, the human Nup84 homolog, in complex with Nup133 is known[17]. Therefore, we were able to model full-length Nup84 based on the experimentally known N- and C-terminal fragments, and the homology-modeled structure of the intervening 84-residue segment using other ACE1 domains (see Methods for details). After Nup84 was positioned, Nup133 could be docked based on the Nup107-Nup133 complex structure[21]. Finally, the last element on the long stalk of the Y-complex is the N-terminal Nup133 β-propeller, which is loosely tethered to the C-terminal, α-helical stack element[16,35]. The resulting composite structure constitutes the conserved, heterohexameric core of the Y-complex (Fig. 3a).

Because the composite model is built from structural elements of four different organisms, we examined to what extent this might affect the overall structure. Therefore, we also built models for the heteroheptameric Y-complex in *S. cerevisiae*, including Seh1, as well as the heterodecameric Y-complex in *H. sapiens*, including Seh1 and Nup37 (Fig. 3b,c). The Seh1 position can be deduced from the Seh1-Nup85 complex structure[18,24], while the Nup37 position is known from the Nup37-Nup120 complex structure[22,36]. The positions of Nup43 and ELYS within the human complex are not well understood and were therefore excluded. By comparison, we observed that the conserved, heterohexameric core changes only in local areas between the three models and that the overall shape and dimensions of the Y-complex appear conserved in all opisthokonts. Organism-specific proteins decorate the Y-core, but do not significantly influence its overall structure otherwise.

Our composite structure reveals that the Y-complex when viewed from the front measures about 20 nm wide and 40 nm high (Fig. 3). This is in good agreement with published EM structures and computational models[15,28,37]. However, the principal angles between the three extensions from the hub deviate significantly between our X-ray based structure and the EM structures, which is evident by superimposing the different sets of data (Fig. 4). Strikingly, when viewed from the side or the top, the composite crystal structure reveals a distinct, three-dimensional shape (Fig. 3e, Fig. 4b,f), while the previously reported structures were essentially flat (Fig. 4d,h). At the hub, the three extensions, namely the two arms and the stalk, exhibit strong curvature and form a dome-shaped structure. As a result, we measure a thickness of ~8 nm for the Y-complex (Fig. 3e), compared to ~4 nm reported in previous EM analyses. Theoretically, this difference could be the result of flexibility within the Y-complex, which is well documented. In our composite structure we can now specify the main hinge regions and flexible areas (Fig. 5). These flexible regions are detected by general considerations regarding protein structure, domain boundaries established by limited proteolysis, and flexibility observed in previous crystallographic and EM studies[15-17,21,22,37]. The hub itself is rather rigid, since four proteins engage in a tightly coordinated interface. To flatten the Y-complex, the helical Nup120 C-terminal domain or the Nup85 ACE1 element would have to bend by nearly 90° with respect to each other. Helical stacks have the propensity to bend, as best exemplified by various nuclear transport receptors[38,39], but the direction of bending is determined by the helical orientation. For the flattening of the Y, the predicted-to-be bendable elements are, however, oriented in an unfavorable way. This means that the necessary distortions in Nup120 or Nup85 would be energetically costly because of the disruption to the hydrophobic core that they would generate, which we consider to be rather unlikely. Therefore, the simplest explanation for the discrepancy between our composite crystal structure and previous random-conical tilt (RCT) negative stain EM structures is that the latter were artificially flattened in the direction normal to the EM grid, a well-known phenomenon.

Implications for NPC assembly models

Next, we tested whether our composite human Y-complex could be positioned into the recently published 3.2 nm cryo-ET density map[15] of the human NPC, which predicted a staggered two-ring, head-to-tail orientation of Y-complexes, symmetrically positioned on the nucleoplasmic and the cytoplasmic face of the NPC. We were able to recapitulate the

published results of docking the flat, Y-complex structure determined by RCT negative stain EM (EMD code 2443)[15] into the cryo-ET map[15]. We then tried the same procedure using our highly curved Y-complex structure. We searched with the human Y-complex model omitting Nup133 and the tail domain (residues 658–925) of Nup107, presumably the most flexible Y-complex elements. Nup133 has an N-terminal β-propeller flexibly connected to a C-terminal helical stack domain[16]. The helical domain of Nup133 is tripartite, with hinges connecting the three helical segments[21]. A flexible hinge in the Nup107 ACE1 element between the trunk-crown, and tail segments can be postulated based on independent structure-mapping studies performed on the human and yeast homologs[17,19,25]. Using this stubbed Y-complex, we found three top numerical solutions (see Methods for details). Two solutions roughly coincided with the outer Y-complex ring postulated by Bui et al.[15] (Fig. 6), and the third solution coincided with the inner ring of that study (Supplementary Fig. 5). While our work was in review, Stuwe et al. reported the docking of a similarly stubbed Y-complex from *S. cerevisiae* based on a 7.4 Å crystal structure, which shows a curved topology consistent with our structure, and arrived at a similar solution[34]. However, when we added the Nup107 tail and Nup133 structures back to the docked Y-complex model of our third solution, in any topologically reasonable way, we observed extensive steric clashes with the neighboring Y-complex that seem highly implausible (Supplementary Fig. 5). Thus, we did not consider this solution further. Regarding the two top solutions, they are rotated around the hub by approximately 20° relative to each other. In each solution the long stalk could be fitted reasonably well to two different regions in the EM density. Both solutions result in a seemingly closed ring when Nup133 is added, albeit the head-to-tail contact would be different in each case. To fit each solution, the long stalk needs to adopt different conformations, largely by adjusting Nup133, which seems realistic based on the expected flexibility around distinct hinge points (Fig. 6c). Obviously, both solutions cannot coexist due to excessive steric clashes. Therefore, the easiest way to explain our docking results is to suggest that the Y-complex ring is a single rather than a double ring, but that it can adopt at least two conformations. We argue that because of subtomogram-averaging, we might see an overlay of the two, equally and most populated, states of the Y-complex ring in the cryo-ET density.

DISCUSSION

As reasonable as our docking attempts may appear, we would like to caution about the interpretation of these results. First, the available cryo-ET map (EMD-2444)[15] is calculated based on assumptions that we still do not know to be necessarily correct. For example, a strict eightfold rotational symmetry is applied, which may be appropriate at nm resolution, but possibly not at atomic resolution. If this symmetry is not true on the atomic level, the calculated map could be intrinsically flawed. Due to the similarity of various scaffold nups on a nanometer scale this is particularly troublesome. Second, docking at ~3 nm resolution is at best tentative and only reasonable to attempt because of the distinct and large size of the Y-complex. It is possible that an entire portion of the Y-complex is so flexible in the NPC assembly that it could simply be averaged out in the cryo-ET study. This could in principal be true for the long stalk as well as most of the Nup120 arm, which can bend perpendicular

to the long axis of its C-terminal helical stack domain[22] . Many additional docking solutions would need to be considered, if such possibilities were entertained.

One way of independently confirming a specific assembly model initially derived from docking is to map the assumed contacts between neighboring complexes. Bui et al. attempted this by crosslinking experiments[15]. Surprisingly, only two such crosslinks (Nup107-Nup133 and Nup43-Nup96) were found. However, these interactions could not be confirmed by additional experiments and, therefore, are insufficient to distinguish between the models. A two-ring model in particular would generate many inter-Y contact sites, thus the paucity of detected crosslinks is unexpected. Taking additional studies into account does not resolve the discrepancy between the reticulated two ring model and a flexible one ring model. For example, the radial distribution of fluorescently labeled scaffold nucleoporins was determined by super-resolution microscopy [40]. However, the raw localization precision of 20-30 nm attained in that study is insufficient to distinguish between the different ring models. Stoichiometric considerations, which have major model implications, are also not definitive. For example, a recent study concluded there are 32 copies of Y-complexes per NPC in HeLa cells[41], a number supporting a two ring model, while earlier studies argued for 16 copies[6,42], which would favor a one ring model. Recent advancements in super-resolution microscopy should allow for the direct counting individual nucleoporins within an NPC, putting this controversy to rest soon[43]. Finally, mass estimates for the NPC range from 40 MDa to 120 MDa, depending on the species and technique used[4-6]. Again, it is premature to use this information to definitively validate a specific model. In conclusion, to confirm any model, additional experimental data that have an appropriate resolution are needed. Interaction data that would confirm contacts between neighboring subcomplexes would likely be the most helpful tool. Regardless, the Y-complex structure presented here at least provides a benchmark that any reasonable model needs to be consistent with.

METHODS

Construct generation

Nup120$_{952-1241}$, Nup145C$_{233-791}$, Nup85$_{257-1181}$, and full-length Sec13 were cloned from *Myceliophthora thermophila (Mt)*. Nup120$_{952-1241}$ was C-terminally fused with a 10xHis tag and cloned into a kanamycin resistant, T7-promoter-based bacterial expression vector. To increase stability, full-length Sec13 was fused C-to-N-terminally to Nup145C$_{147-705}$ using a flexible four-residue linker, in analogy to a previously described *S. cerevisiae* construct[19]. The Sec13-Nup145C fusion was N-terminally tethered to a 3C protease cleavable SUMO tag and cloned into an ampicillin resistant, T7-promoter-based bacterial expression vector. Nup85$_{257-1181}$ was N-terminally fused with a 3C protease cleavable 10xHis-8xArg-SUMO tag. The tetrameric complex is referred to as Nup120-Sec13-Nup145C-Nup85 for simplicity.

Protein production and purification

Nup120 and Sec13-Nup145C vectors were co-transformed into *Escherichia coli* LOBSTR-RIL(DE3) (Kerafast)[44] cells and protein production was induced with 0.2 mM IPTG at 18 °C for 12-14 h. Nup85 was expressed separately under identical conditions. Cells were

collected by centrifugation at 6,000g, resuspended in lysis buffer (50 mM potassium phosphate (pH 8.0), 500 mM NaCl, 30 mM imidazole, 3 mM β-mercaptoethanol (βME), 1 mM PMSF) and lysed using a cell disruptor (Constant Systems). The lysate was cleared by centrifugation at 12,500g for 15min. The soluble fraction was incubated with Ni Sepharose 6 Fast Flow beads (GE Healthcare) for 30min on ice. After washing the beads with lysis buffer the protein was eluted (250 mM imidazole, pH8.0, 150 mM NaCl, 3 mM βME). The Nup85 Ni-eluate was diluted 1:1 with 20 mM Hepes·KOH (pH 7.4), 0.1 mM EDTA, 1 mM dithiothreitol (DTT) and subjected to cation exchange chromatography on a HiTrapS column (GE Healthcare) using a linear NaCl gradient. The Nup120-Sec13-Nup145C Ni-eluate was incubated with 3C and dialyzed overnight at 4 °C (20 mM Hepes·KOH (pH 7.4), 150 mM NaCl, 0.1 mM EDTA, 1 mM DTT). Both samples were further purified separately via size exclusion chromatography on a Superdex S200 16/60 column (GE Healthcare) equilibrated in running buffer (10 mM Tris·HCl (pH 8.0), 150 mM NaCl, 1 mM NaCl, 1mM DTT). Purified 10xHis-8xArg-SUMO-Nup85 was incubated with an excess of purified Nup120-Sec13-Nup145C and the assembled quaternary complex was separated via cation-exchange chromatography. Nup120-Sec13-Nup145C-Nup85 complex was incubated with 3C overnight at 4 °C and subjected to a final purification by size exclusion chromatography on Superdex S200 (GE Healthcare). Selenomethionine (SeMet) derivatized Nup85 and Nup120-Sec13-Nup145C-Nup85 was prepared as described previously[18] and purified as the native version, except that the reducing agent concentration (βME, DTT) was 5 mM in all buffers.

Crystallization

Initial crystals of Nup120-Sec13-Nup145C-Nup85 were obtained at 18 °C in 9 days in sitting drops over a reservoir containing 50 mM Tris·HCl (pH 8.5), 1 M NH_4SO_4. 10 mM EDTA as an additive reduced nucleation and improved the shape of the crystals. Hanging drops of 1 μl protein at 3 mg/ml and 1 μl of precipitant (50 mM Tris·HCl (pH 8.23), 0.7 M $(NH_4)_2SO_4$, 20 mM EDTA) were supplemented on the third day of incubation with 0.2 μl seed stock to yield diffraction quality, thin triangular plates. Selenomethionine-derivatized protein crystallized under identical conditions. Crystals were cryo-protected in mother liquor supplemented with 20 % (v/v) ethylene glycol.

Data collection and structure determination

Data collection was performed at the Advanced Photon Source end station 24-IDC. All data processing steps were carried out with programs provided through SBgrid[45]. Data reduction was performed using HKL2000[46]. Sec13 from *S. cerevisiae* (3MZK, chain A)[29] was used as a search model for molecular replacement (MR). One unique solution was found in a Nup85-only SeMet derivative (space group $P2_1$, 1 copy per asymmetric unit). Partial MR phases were then used to find 12 out of 20 possible SeMet positions (8 were in disordered regions) with *Phaser* within the PHENIX suite[47] using the MR-single anomalous dispersion (MR-SAD) protocol. An interpretable 4.1Å experimental electron density map was obtained after solvent modification using *Parrot* from the CCP4 suite[48]. The backbone of most of the model was traced and the sequence for Nup85 was assigned, aided by the selenium positions as markers and the partial Nup85 models available (PDB codes: 3EWE, 3F3F)[18,24] Next, this initial model was used as a search model for MR with the dataset obtained from fully

SeMet-derivatized protein (space group P1, two copies per asymmetric unit). Two unambiguous solutions were readily found using *Phaser.* Again, MR-SAD was used to find 36 selenium sites (out of 74 possible, with 26 in disordered regions), which served as markers to assign the sequence for Nup120 and Nup145C. To build *mt*Sec13, a starting model was generated using *Rosetta*[49] and Sec13 from *S. cerevisiae* (62% sequence identity). Model building was carried out with *Coot*[50] and *phenix.refine* was used for refinement. NCS and secondary structure restraints were applied throughout the refinement process. For the final refined structure, Ramachandran values were: 91% favored, 8.2% allowed, and 0.8% outlier. The *MolProbity*[51] clashscore was 8.33 and the *MolProbity* percentile was 97%.

Generation of Y-complex composite structures

A composite structure of the minimal, hexameric Y-complex was generated in *Coot* using secondary structure match (SSM) superposition of solved, overlapping crystal structure fragments. Nup85, Sec13, and the Nup120 tail coordinates are the *M. thermophila* orthologs and are from this study. $Nup120_{1-948}$ from *S. pombe* (sp) (PDB code: 4FHM)[22] was used to generate a full-length hybrid Nup120 structure together with the Mt fragment. Nup145C is a hybrid structure with the trunk and tail domains from Mt (this study) and the crown domain from *S. cerevisiae*, which allowed for the confident modeling of the Nup145C-Nup84 junction previously solved in *S. cerevisiae* (PDB code: 3JRO, 3IKO)[19,25]. Nup84 is a hybrid structure: with the crown and trunk domains from *S. cerevisiae* (PDB code: 3JRO)[19] and the tail domain from the *H. sapiens* Nup107 ortholog (PDB code: 3I4R)[21]. Four helices between the trunk and tail domains on Nup84 were modeled from the corresponding helices solved in Nic96 (PDB code: 2QX5, 2RFO)[52,53] using Phyre2 one-to-one threading[54]. Nic96 was chosen as the template because superposition between its trunk and tail domains and the corresponding regions on Nup84 yielded the lowest RMSD of all solved ACE1 domain proteins. Additionally, the *BackPhyre*[54] structure prediction server suggests that Nic96 is the closest Nup homolog to Nup84 and vice versa, despite low sequence identity of 8%. The Nup133 stacked α-helical domain and its junction with Nup107 are from *H. sapiens* (PDB code: 3I4R)[21]. The interface between the Nup133 β-propeller (PDB code: 1XKS)[16] and the stacked α-helical domain is not known but is expected to be flexible, based on limited proteolysis data (data not shown).

Composite structures of the heptameric *S. cerevisiae* and the octameric *H. sapiens* Y-complexes were generated in *Coot* using SSM superposition onto the minimal composite structure of solved and modeled structure fragments generated by one-to-one threading with the program *Phyre2*. For the *S. cerevisiae* Y-complex composite, $scNup120_{714-1036}$ was modeled with spNup120 (PDB code: 4FHM)[22] as the template. $scNup85_{495-744}$ was modeled with mtNup85. $scNup145C_{534-712}$ was models with mtNup145C. scNup133 was modeled with hsNup133 (PDB code: 1XKS, 3I4R)[16,21]. $scNup84_{425-726}$ was modeled with hsNup107 and scNic96 as described above. For the human Y-complex composite, hsNup160 was modeled with spNup120 (PDB code: 4FHM)[22] as the template. $hsNup85_{1-411}$ was modeled with scNup85 (PDB codes: 3EWE, 3F3F)[18,24]. $hsNup85_{415-652}$ was modeled with mtNup85. $hsNup96_{1-732}$ was modeled with scNup145C (PDB code: 3JRO, 3IKO)[19,25]. $hsNup96_{733-937}$ was modeled with mtNup145C. $hsNup107_{1-657}$ was modeled with scNup84 and scNic96 as described above. The composite structures are available upon request.

Fitting composite Y-complex structures into single particle 3-D reconstruction EM maps of Y-complexes

Composite *H. sapiens* (omitting Nup133 and Nup107$_{658-925}$) *and S. cerevisiae* Y-complex structures were fitted into the published EM maps for the respective species (EMD codes: 2443, 5152)[15] using the Fitmap tool from *Chimera*[55]. 1000 trials were run with an apparent resolution of 33 Å for human and 35 Å for the *S. cerevisiae* composite structure. For fitting the human composite model into EMD-2443[15], the best solution had a correlation score of 0.8235 with 116/1000 hits (Fig. 4c). The next best solution (not shown) had a correlation score of 0.8219 with 8/1000 hits. For fitting the yeast composite model into EMD-5152[15], the best solution had a correlation score of 0.6992 with 18/1000 hits (Fig. 4g). The next best solution (not shown) had a correlation score of 0.6374 with 19/1000 hits.

Fitting composite *H. sapiens* and *S. cerevisiae* Y-complex structures into 3-D reconstruction EM tomography map of the entire NPC

A procedure similar to the one outlined in Bui et al.[15] was followed to fit both human and yeast composite Y-complex structures into the published EM map of the human NPC (EMD code: 2444)[15] using *Chimera*. To highlight features that are invariant between the cytoplasmic and nuclear ring, a consensus map was generated by multiplication of a binarized copy rotated by 180 degrees with respect to the original EM map, as in Bui et al.[15]. Subsequently, a membrane mask was constructed and subtracted, resulting in a membrane free consensus map, which was used for all fitting calculations. To avoid excluding alternate conformations resulting from flexibility of the long stalk of the Y-complex, Nup133 was omitted from the computational fitting procedure and was fitted manually. 30000 trials were run with an apparent resolution of 35 Å for both human and yeast composite Y-complex structures. For the human composite model, the best solution (conformation 1, Fig. 6b) had a correlation score of 0.7918 with 179/30000 hits. The second best solution (conformation 2, Fig. 6b) had a correlation score of 0.7661 with 252/30000 hits. The third best solution (inner ring, fig. S8) had a correlation score of 0.7516 with 94/30000 hits. Other lower scoring solutions were not considered further based on steric considerations. Similar results were obtained when using the yeast composite Y-complex structure as a search model.

Multiple sequence alignment generation

Multiple sequence alignments were generated for all components of the hub structure using sequences representative of the eukaryotic tree of life[56,57]. Sequences, except for Nup85 and Nup120, were obtained via *BLAST* searches and aligned using *Muscle* in *JalView*[58]. Nup85 and Nup120 multiple sequence alignments were obtained from ref. 9, pruned, and realigned using *ClustalW*.

Yeast Plasmid Construction

The entire *NUP145*, *NUP85*, and *NUP120* genes with their endogenous promoters and terminators (~1000 nucleotides before the start codon and ~400 after the stop codon, respectively) were separately cloned into the multiple cloning site of the centromeric YCplac33 shuttle vector. Additionally, the entire *NUP145* and *NUP85* genes with their

endogenous promoters and terminators were separately cloned into the multiple cloning site of the centromeric prs315 vector. All cloning was performed following the standard Gibson assembly method[59]. The constructed wild type vectors used in this study were named as follows: GKYp01 (*NUP120*, *URA3*, *CEN*), GKYp02 (*NUP85*, *URA3*, *CEN*), GKYp03 (*NUP145*, *URA3*, *CEN*), GKYp04 (*NUP85*, *LEU2*, *CEN*), and GKYp05 (*NUP145*, *LEU2*, *CEN*).

Vectors where the last C-terminal alpha helix of Nup120 (α30, 1016-1037), Nup85 (α30, 719-744), and Nup145C (α27, 689-712) has been deleted were also generated using GKYp01, GKYp04, and GKYp05, respectively. The deletion vectors were created by introducing an early stop codon using the Quikchange site-directed mutagenesis method. The constructed deletion vectors used in this study were named as follows: GKYp06 (*NUP120* α30, *URA3*, *CEN*), GKYp07 (*NUP85* α30, *LEU2*, *CEN*), and GKYp08 (*NUP145* α27, *LEU2*, *CEN*).

Yeast Strain Construction

Yeast strains used in this study are listed in Supplementary Table 3. The *NUP120* haploid strain was obtained from the *S. cerevisiae* deletion consortium (background BY4742, #14906), transformed with either the YCplac33 empty vector (negative control), GKYp01 (positive control), or GKYp06 (truncation), and selected on plates lacking uracil. The diploid *NUP85* and *NUP145* strains were also obtained from the *S. cerevisiae* deletion consortium (background BY4743, #26840 and #24459, respectively), transformed with either GKYp02 or GKYp03, respectively, and selected on uracil negative plates. The transformed diploids were then sporulated and subjected to tetrad dissection. The resulting *NUP85* haploids containing GKYp02 were transformed with either prs315 empty vector (negative control), GKYp04 (positive control), or GKYp07 (truncation), while the *NUP145* haploids containing GKYp03 were transformed with either prs315 empty vector (negative control), GKYp05 (positive control), or GKYp08 (truncation). The *NUP85* and *NUP145* haploid transformations were selected on plates lacking leucine.

Cell Growth Analysis

The *NUP120* strains containing YCplac33, GKYp01, or GKYp06 were grown as a liquid culture in YPD overnight shaking at 30 °C. The cultures were then diluted in YPD to an OD_{600} of 0.1 and aliquoted into a 96-well plate (100 μl of culture / well). The plate was placed into a Synergy 2 multi-mode microplate reader (BioTek) and the OD_{600} of all the wells containing a culture were monitored every 15 min for 24 h. The plate was shook continuously and kept at 30 °C.

The *NUP85* haploid strains containing GKYp02 and prs315, GKY04, or GKY07 and the *NUP145* haploid strains containing GKYp03 and prs315, GKY05, or GKY08 were grown as a liquid culture in YPD overnight shaking at 30 °C. The cultures were then diluted in either SC medium (containing all 20 amino acids, uracil and 2% glucose) or SC medium containing 5-fluoroorotic acid (5-FOA) at 1 mg/ml. The plate was placed into a Synergy 2 multi-mode microplate reader and the OD_{600} of all the wells containing a culture were monitored every 15 min for 24 h. The plate was shook continuously and kept at 30 °C.

The growth of three separate clones of each strain was tested in quintuplicates. The data was graphed in Prism (GraphPad Software). All error bars represent the standard deviation of the mean.

Supplementary Material

Refer to Web version on PubMed Central for supplementary material.

ACKNOWLEDGEMENTS

References

1. Hetzer MW, Wente SR. Border control at the nucleus: biogenesis and organization of the nuclear membrane and pore complexes. Dev. Cell. 2009; 17:606–616. [PubMed: 19922866]

2. Strambio-de-Castillia C, Niepel M, Rout MP. The nuclear pore complex: bridging nuclear transport and gene regulation. Nat. Rev. Mol. Cell. Biol. 2010; 11:490–501. [PubMed: 20571586]

3. Brohawn SG, Partridge JR, Whittle JRR, Schwartz TU. The nuclear pore complex has entered the atomic age. Structure. 2009; 17:1156–1168. [PubMed: 19748337]

4. Reichelt R, et al. Correlation between structure and mass distribution of the nuclear pore complex and of distinct pore complex components. J. Cell Biol. 1990; 110:883–894. [PubMed: 2324201]

5. Yang Q, Rout MP, Akey CW. Three-dimensional architecture of the isolated yeast nuclear pore complex: functional and evolutionary implications. Mol. Cell. 1998; 1:223–234. [PubMed: 9659919]

6. Rout MP, et al. The yeast nuclear pore complex: composition, architecture, and transport mechanism. J. Cell Biol. 2000; 148:635–651. [PubMed: 10684247]

7. Walther TC, et al. The conserved Nup107-160 complex is critical for nuclear pore complex assembly. Cell. 2003; 113:195–206. [PubMed: 12705868]

8. Harel A, et al. Removal of a single pore subcomplex results in vertebrate nuclei devoid of nuclear pores. Mol. Cell. 2003; 11:853–864. [PubMed: 12718872]

9. Lutzmann M, Kunze R, Buerer A, Aebi U, Hurt E. Modular self-assembly of a Y-shaped multiprotein complex from seven nucleoporins. EMBO J. 2002; 21:387–397. [PubMed: 11823431]

10. Belgareh N, et al. An evolutionarily conserved NPC subcomplex, which redistributes in part to kinetochores in mammalian cells. J. Cell Biol. 2001; 154:1147–1160. [PubMed: 11564755]

11. Vasu S, et al. Novel vertebrate nucleoporins Nup133 and Nup160 play a role in mRNA export. J. Cell Biol. 2001; 155:339–354. [PubMed: 11684705]

12. Neumann N, Lundin D, Poole AM. Comparative genomic evidence for a complete nuclear pore complex in the last eukaryotic common ancestor. PLoS ONE. 2010; 5:e13241. [PubMed: 20949036]

13. Vollmer B, Antonin W. The diverse roles of the Nup93/Nic96 complex proteins - structural scaffolds of the nuclear pore complex with additional cellular functions. Biol. Chem. 2014; 395:515–528. [PubMed: 24572986]

14. Alber F, et al. The molecular architecture of the nuclear pore complex. Nature. 2007; 450:695–701. [PubMed: 18046406]

15. Bui KH, et al. Integrated structural analysis of the human nuclear pore complex scaffold. Cell. 2013; 155:1233–1243. [PubMed: 24315095]

16. Berke IC, Boehmer T, Blobel G, Schwartz TU. Structural and functional analysis of Nup133 domains reveals modular building blocks of the nuclear pore complex. J. Cell Biol. 2004; 167:591–597. [PubMed: 15557116]

17. Boehmer T, Jeudy S, Berke IC, Schwartz TU. Structural and functional studies of Nup107/Nup133 interaction and its implications for the architecture of the nuclear pore complex. Mol. Cell. 2008; 30:721–731. [PubMed: 18570875]

18. Brohawn SG, Leksa NC, Spear ED, Rajashankar KR, Schwartz TU. Structural evidence for common ancestry of the nuclear pore complex and vesicle coats. Science. 2008; 322:1369–1373. [PubMed: 18974315]

19. Brohawn SG, Schwartz TU. Molecular architecture of the Nup84-Nup145C-Sec13 edge element in the nuclear pore complex lattice. Nat. Struct. Mol. Biol. 2009; 16:1173–1177. [PubMed: 19855394]

20. Leksa NC, Brohawn SG, Schwartz TU. The structure of the scaffold nucleoporin Nup120 reveals a new and unexpected domain architecture. Structure. 2009; 17:1082–1091. [PubMed: 19576787]

21. Whittle JRR, Schwartz TU. Architectural nucleoporins Nup157/170 and Nup133 are structurally related and descend from a second ancestral element. J. Biol. Chem. 2009; 284:28442–28452. [PubMed: 19674973]

22. Bilokapic S, Schwartz TU. Molecular basis for Nup37 and ELY5/ELYS recruitment to the nuclear pore complex. Proc. Natl. Acad. Sci. USA. 2012; 109:15241–15246. [PubMed: 22955883]

23. Hsia K-C, Stavropoulos P, Blobel G, Hoelz A. Architecture of a coat for the nuclear pore membrane. Cell. 2007; 131:1313–1326. [PubMed: 18160040]

24. Debler EW, et al. A fence-like coat for the nuclear pore membrane. Mol. Cell. 2008; 32:815–826. [PubMed: 19111661]

25. Nagy V, et al. Structure of a trimeric nucleoporin complex reveals alternate oligomerization states. Proc. Natl. Acad. Sci. USA. 2009; 106:17693–17698. [PubMed: 19805193]

26. Seo H-S, et al. Structural and functional analysis of Nup120 suggests ring formation of the Nup84 complex. Proc. Natl. Acad. Sci. USA. 2009; 106:14281–14286. [PubMed: 19706512]

27. Sampathkumar P, et al. Structure of the C-terminal domain of Saccharomyces cerevisiae Nup133, a component of the nuclear pore complex. Proteins. 2011; 79:1672–1677. [PubMed: 21365675]

28. Fernandez-Martinez J, et al. Structure-function mapping of a heptameric module in the nuclear pore complex. J. Cell Biol. 2012; 196:419–434. [PubMed: 22331846]

29. Whittle JRR, Schwartz TU. Structure of the Sec13-Sec16 edge element, a template for assembly of the COPII vesicle coat. J. Cell Biol. 2010; 190:347–361. [PubMed: 20696705]

30. Thierbach K, et al. Protein interfaces of the conserved Nup84 complex from Chaetomium thermophilum shown by crosslinking mass spectrometry and electron microscopy. Structure. 2013; 21:1672–1682. [PubMed: 23954503]

31. Spear ED. A Tumor suppressor complex with GAP activity for the Rag GTPases that signal amino acid sufficiency to mTORC1. Science. 2013; 340:1100–1106. [PubMed: 23723238]

32. Algret R, et al. Molecular architecture and function of the SEA complex, a modulator of the TORC1 pathway. Mol. Cell. Proteomics. 2014; 13:2855–2870. [PubMed: 25073740]

33. Siniossoglou S, et al. A novel complex of nucleoporins, which includes Sec13p and a Sec13p homolog, is essential for normal nuclear pores. Cell. 1996; 84:265–275. [PubMed: 8565072]

34. Stuwe T, et al. Architecture of the nuclear pore complex coat. Science. 2015:1–7. doi:10.1126/science.aaa4136.

35. Kim SJ, et al. Integrative structure-function mapping of the nucleoporin Nup133 suggests a conserved mechanism for membrane anchoring of the nuclear pore complex. Mol. Cell. Proteomics. 2014; 13:2911–2926. [PubMed: 25139911]

36. Liu X, Mitchell JM, Wozniak RW, Blobel G, Fan J. Structural evolution of the membrane-coating module of the nuclear pore complex. Proc. Natl. Acad. Sci. USA. 2012; 109:16498–16503. [PubMed: 23019579]

37. Kampmann M, Blobel G. Three-dimensional structure and flexibility of a membrane-coating module of the nuclear pore complex. Nat. Struct. Mol. Biol. 2009; 16:782–788. [PubMed: 19503077]

38. Süel KE, Cansizoglu AE, Chook YM. Atomic resolution structures in nuclear transport. Methods. 2006; 39:342–355. [PubMed: 16938467]

39. Cook A, Bono F, Jinek M, Conti E. Structural biology of nucleocytoplasmic transport. Annu Rev Biochem. 2007; 76:647–671. [PubMed: 17506639]

40. Szymborska A, et al. Nuclear pore scaffold structure analyzed by super-resolution microscopy and particle averaging. Science. 2013; 341:655–658. [PubMed: 23845946]

41. Ori A, et al. Cell type-specific nuclear pores: a case in point for context-dependent stoichiometry of molecular machines. Mol. Syst. Biol. 2013; 9:648. [PubMed: 23511206]

42. Cronshaw JM, Krutchinsky AN, Zhang W, Chait BT, Matunis MJ. Proteomic analysis of the mammalian nuclear pore complex. J. Cell Biol. 2002; 158:915–927. [PubMed: 12196509]

43. Ries J, Kaplan C, Platonova E, Eghlidi H, Ewers H. A simple, versatile method for GFP-based super-resolution microscopy via nanobodies. Nat. Methods. 2012; 9:582–584. [PubMed: 22543348]

44. Andersen KR, Leksa NC, Schwartz TU. Optimized E. coli expression strain LOBSTR eliminates common contaminants from His-tag purification. Proteins. 2013; 81:1857–1861. [PubMed: 23852738]

45. Morin A, et al. Collaboration gets the most out of software. eLife. 2013; 2:e01456–e01456. [PubMed: 24040512]

46. Otwinowski Z, Minor W. Processing of X-ray diffraction data collected in oscillation mode. Meth. Enzymol. 1997; 276:307–326.

47. Adams PD, et al. PHENIX: a comprehensive Python-based system for macromolecular structure solution. Acta Crystallogr. D Biol. Crystallogr. 2010; 66:213–221. [PubMed: 20124702]

48. Winn MD, et al. Overview of the CCP4 suite and current developments. Acta Crystallogr. D Biol. Crystallogr. 2011; 67:235–242. [PubMed: 21460441]

49. Terwilliger TC, et al. phenix.mr_rosetta: molecular replacement and model rebuilding with Phenix and Rosetta. J. Struct. Funct. Genomics. 2012; 13:81–90. [PubMed: 22418934]

50. Emsley P, Lohkamp B, Scott WG, Cowtan K. Features and development of Coot. Acta Crystallogr. D Biol. Crystallogr. 2010; 66:486–501. [PubMed: 20383002]

51. Chen VB, et al. MolProbity: all-atom structure validation for macromolecular crystallography. Acta Crystallogr. D Biol. Crystallogr. 2010; 66:12–21. [PubMed: 20057044]

52. Jeudy S, Schwartz TU. Crystal structure of nucleoporin Nic96 reveals a novel, intricate helical domain architecture. J. Biol. Chem. 2007; 282:34904–34912. [PubMed: 17897938]

53. Schrader N, et al. Structural basis of the nic96 subcomplex organization in the nuclear pore channel. Mol. Cell. 2008; 29:46–55. [PubMed: 18206968]

54. Kelley LA, Sternberg MJE. Protein structure prediction on the Web: a case study using the Phyre server. Nat Protoc. 2009; 4:363–371. [PubMed: 19247286]

55. Pettersen EF, et al. UCSF Chimera--a visualization system for exploratory research and analysis. J Comput Chem. 2004; 25:1605–1612. [PubMed: 15264254]

56. Ciccarelli FD, et al. Toward automatic reconstruction of a highly resolved tree of life. Science. 2006; 311:1283–1287. [PubMed: 16513982]

57. Fritz-Laylin LK, et al. The genome of Naegleria gruberi illuminates early eukaryotic versatility. Cell. 2010; 140:631–642. [PubMed: 20211133]

58. Waterhouse AM, et al. Jalview Version 2--a multiple sequence alignment editor and analysis workbench. Bioinformatics. 2009; 25:1189–1191. [PubMed: 19151095]

59. Gibson DG, et al. Enzymatic assembly of DNA molecules up to several hundred kilobases. Nat. Methods. 2009; 6:343–345. [PubMed: 19363495]
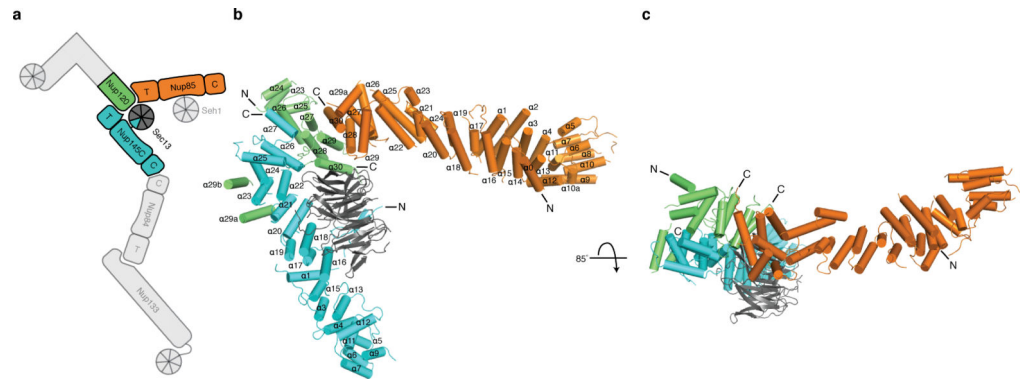
Figure 1. Structure of the *Myceliophthora thermophila* Y-complex hub at 4.1 Å resolution
(**a**) Schematic of the Y-complex. Regions included in the crystallization construct are colored, other Y-complex regions in grey. Elements of ACE1 fold proteins are indicated: T – tail and C – crown flank the central trunk element. (**b**) The hub structure is colored as follows: Nup85 (orange), Nup120 (green), Nup145C (cyan), and the Sec13 β-propeller (grey). N and C termini are indicated for the helical proteins. Helices are numbered according to previously solved *S. cerevisiae* fragments[18,19,22]. Numbers that include a letter modifier indicate helical elements not present in *S. cerevisiae*. (**c**) Top-down view of the hub. The N terminus of Nup145C is not indicated because it is obscured by the 85° rotation.
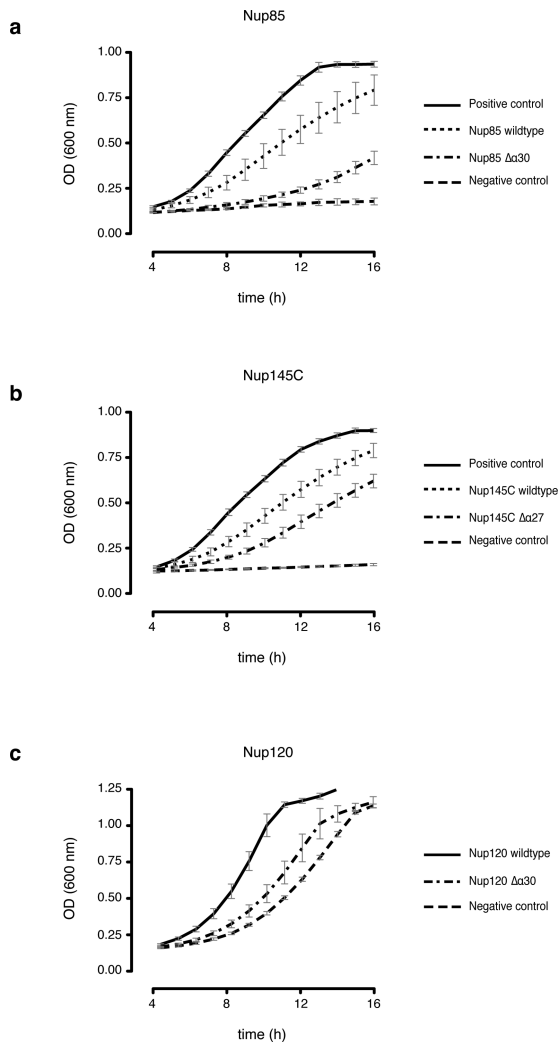
Figure 2. Fitness analysis of hub interactions
(**a**) Growth curves of *NUP85* strains carrying *NUP85:URA3* and either empty pRS315 (negative control), Nup85 wildtype, or Nup85 Δα30 grown in the presence of 5-FOA. The positive control is the *NUP85* strain carrying *NUP85/URA3* and empty pRS315 grown in the absence of 5-FOA. (**b**) Growth curves of *NUP145* strains carrying *NUP145/URA3* and either empty pRS315 (negative control), Nup145C wildtype, or Nup145C Δα27 grown in the presence of 5-FOA. The positive control is the *NUP145* strain carrying *NUP145/URA3* and empty pRS315 grown in the absence of 5-FOA. (**c**) The growth curves of *NUP120* strains carrying YClac33 empty vector (negative control), Nup120 wildtype, or Nup120 Δα30 grown in YPD. Four technical replicates (*n*=4 OD measurements) for each of three biological replicates (*n*=3), from separate colonies, were performed at 30 °C for all experiments. All error bars are standard deviation of the mean (s.e.m.).
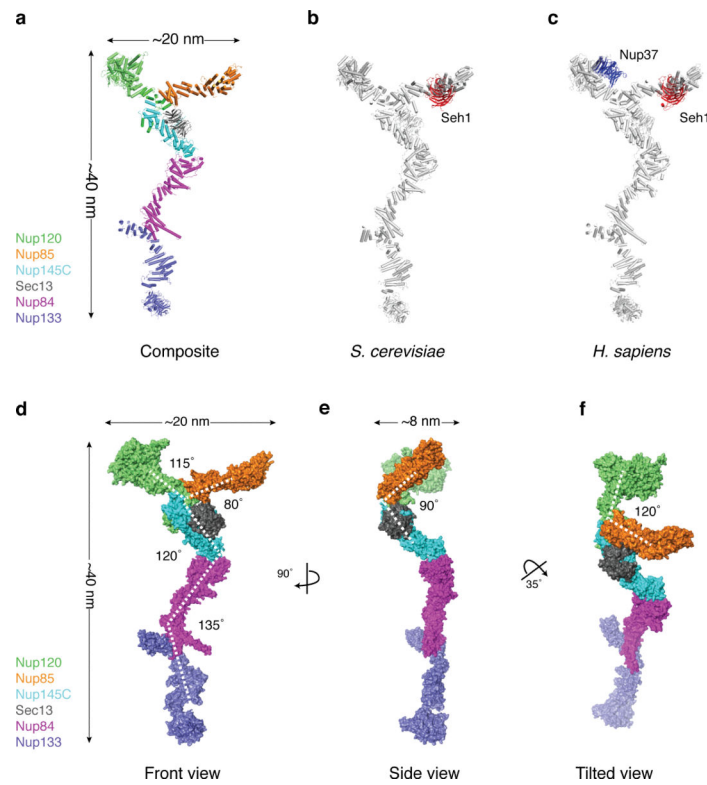
Figure 3. Composite high-resolution structure of the Y-complex
(**a**) Composite, hexameric Y-complex core constructed from the hub structure (Fig. 1) combined with previously published X-ray crystal structure fragments. Within Nup84, 4 helices were modeled computationally. (**b**) Composite *S. cerevisiae* Y-complex based on A), with *S. cerevisiae* sequences threaded onto existing homologous structures. Compared to the universally conserved hexameric Y-complex core shown in A), Seh1 (red) is an additional component found in many organisms, including yeast. (**c**) Composite *H. sapiens* Y-complex with *H. sapiens* sequences threaded onto existing homologous structures. Nup37 (blue) is another Y-complex component only found in a subset of eukaryotes, including humans[12]. (**d**) Space filling surface view of the composite, hexameric Y-complex viewed from the front. (**e**) Side view. (**f**) Tilted view.
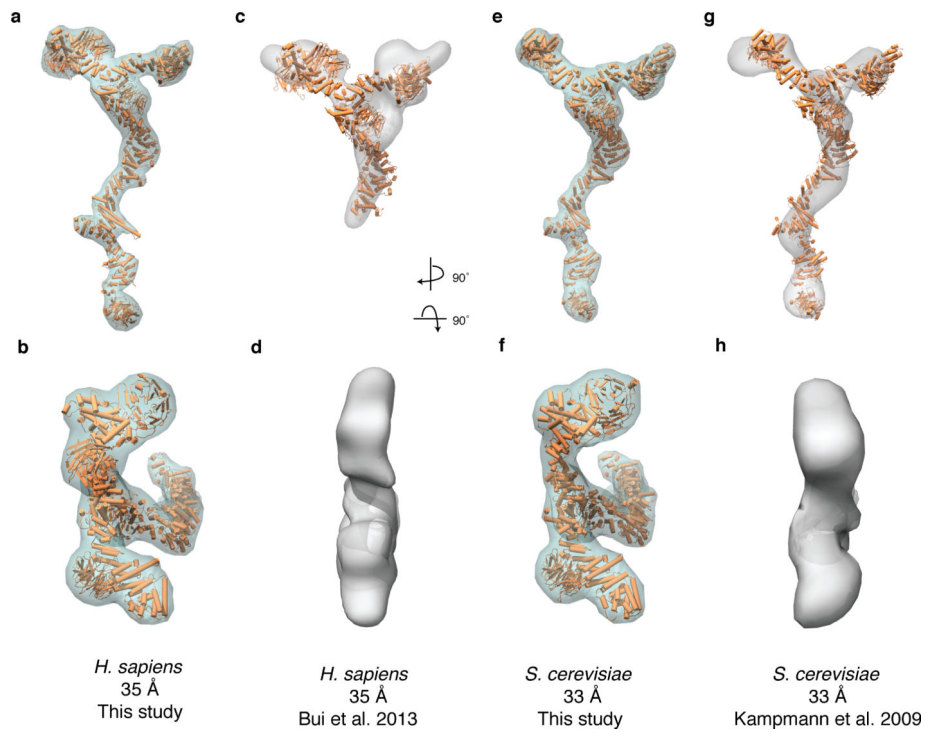
Figure 4. Comparison of the X-ray based, composite Y-complex structure with published 3-D EM reconstruction structures

(**a,b**) Electron density envelope around the composite *H. sapiens* Y-complex calculated for 35 Å resolution from front (a) or top (b) view. (**c,d**) 3-D EM reconstruction of the *H. sapiens* Y-complex with an overlay of the composite model, fitted computationally from front (c) or top (d) view. (**e,f**)Electron density envelope around the composite *S. cerevisiae* Y-complex calculated at 33 Å resolution from front (e) or top (f) view. (**g,h**) 3-D EM reconstruction of the *S. cerevisiae* Y-complex with an overlay of the composite model, fitted computationally from front (g) or top (h) view.
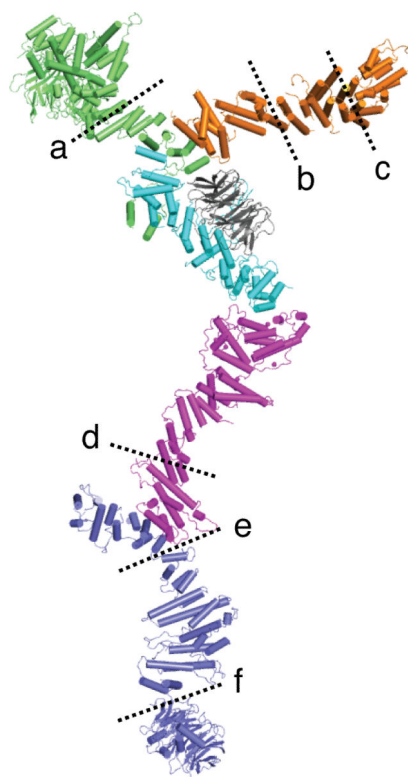
Figure 5. Flexibility of the Y-complex

Experimentally observed hinge regions of the Y-complex are denoted by dashed lines. (**a**) ref. 22. (**b–c**) ref. 18. (**d–e**), refs. 15-17,21,37. (**f**) ref. 16.
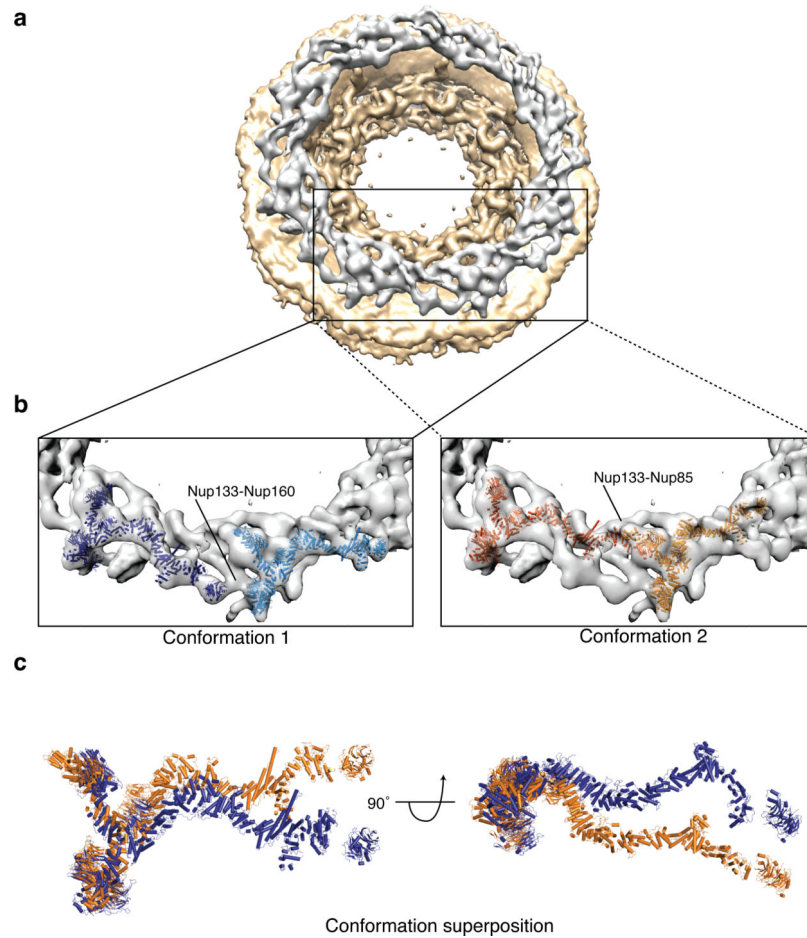
Figure 6. Fitting of the composite *H. sapiens* Y-complex into the cryo-ET map of the entire NPC
(**a**) Consensus map calculated from the cryo-ET map of the human NPC (EMD code: 2444)[15]. The cytoplasmic ring density is highlighted in grey for clarity. (**b**) The top scoring fit of the composite *H. sapiens* Y-complex (conformation 1) and the second top scoring fit (conformation 2) are depicted. (**c**) A superposition of the two fits from (b) shows that they are related by a ~20° rotation about the Y-complex hub, and substantial bending of the long stack.

Table 1

Data collection and refinement statistics

	Nup85(SeMet)$_{257-1181}$, Nup120$_{952-1241}$, Sec13-Nup145C$_{233-791}$	Nup85(SeMet)$_{257-1181}$, Nup120(SeMet)$_{952-1241}$, Sec13-Nup145C(SeMet)$_{233-791}$
Data collection		
Space group	C2	P1
Cell dimensions		
a, b, c (Å)	104.98, 212.02, 170.64	118.96, 107.67, 163.09
α, β, γ (°)	90, 107.2, 90	74.3, 80.4, 63.2
Resolution (Å)	163 - 4.10 (4.25 - 4.10)[a]	157 - 4.00 (4.14 - 4.00)
R_{sym}	0.19 (1.00)	0.21 (0.97)
$I / \sigma I$	8.9 (0.9)	5.3 (0.8)
Completeness (%)	98.2 (93.5)	90.3 (81.3)
Redundancy	6.1 (4.7)	3.6 (2.9)
Refinement		
Resolution (Å)	163 - 4.10	
No. reflections	53648	
R_{work} / R_{free}	31.9/35.8	
No. atoms	10070	
Protein	10070	
Ligand/ion	0	
Water	0	
B factors		
Protein	161.7	
Ligand/ion	0	
Water	0	
r.m.s. deviations		
Bond lengths (Å)	0.002	
Bond angles (°)	0.64	

[a]Values in parentheses are for highest-resolution shell. One crystal was used for each dataset.